

Tuning Legged Locomotion Controllers via Safe Bayesian Optimization

Anonymous Author(s)

Affiliation

Address

email

Abstract:

In this paper, we present a data-driven strategy to simplify the deployment of model-based controllers in legged robotic hardware platforms. Our approach leverages a model-free safe learning algorithm to automate the tuning of control gains, addressing the mismatch between the simplified model used in the control formulation and the real system. This method substantially mitigates the risk of hazardous interactions with the robot by sample-efficiently optimizing parameters within a probably safe region. Additionally, we extend the applicability of our approach to incorporate the different gait parameters as contexts, leading to a safe, sample-efficient exploration algorithm capable of tuning a motion controller for diverse gait patterns. We validate our method through simulation and hardware experiments, where we demonstrate that the algorithm obtains superior performance on tuning a model-based motion controller for multiple gaits safely.

1 Introduction

A model-based control approach can produce highly dynamic and diverse motions for legged robots. This strategy enables rapid adjustment to different robots and bypasses the need for offline training, consequently accelerating the design and testing stages. Nonetheless, it requires an accurate dynamics model of the system, which is often unavailable due to our limited understanding of real-world physics and inevitable simplifications to reduce the computational burden. Consequently, these controllers typically underperform when applied directly to hardware, requiring significant parameter fine-tuning. This tuning process is time-consuming and can also harm the hardware platform. Furthermore, it often needs repetition for different environments or motion patterns to ensure consistent performance across a variety of settings.

This work explores the challenge of identifying optimal control gain parameters for a model-based controller that improves the robustness and tracking performance by bridging the gap between simplified models and real-world dynamics. For this purpose, we utilize GOSAFEOPT [1] to automate the parameter tuning process, enabling the online identification of optimal control gain parameters within a safe region, efficiently utilizing samples and thus safeguarding the hardware platforms during optimization. Furthermore, we extend GOSAFEOPT to incorporate the different gait parameters as contexts. This enables sample-efficient learning of control gains across different gaits. For the resulting contextual GOSAFEOPT algorithm, we give theoretical safety and optimality guarantees.

We demonstrate our method on the quadruped robot *Unitree Go1* [2] in both simulation and hardware experiments. This corresponds to a six dimensional tuning task with a five dimensional context. In the simulation, we show that contextual GOSAFEOPT outperforms other model-free safe exploration

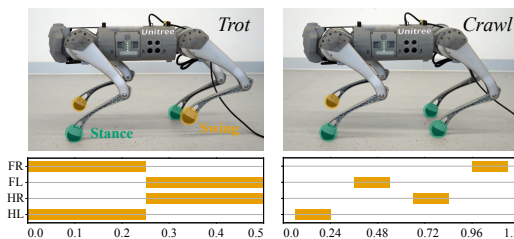


Figure 1: Snapshots of the *Unitree Go1* robot performing *Trot* (left) and *crawl* gaits (right).

40 baselines while making *no unsafe* interactions. Moreover, when trained for different gait patterns,
41 our results clearly indicate that including the gaits as contexts, results in a considerable performance
42 boost. In our hardware experiments, we show that contextual GOSAFEOPT finds optimal feedback
43 controller gains for both the trot and crawl gaits in only 50 learning steps, each while having *no*
44 *unsafe interaction with the real robot*.

45 In summary, the main contributions of this work are as follows; (i) we formulate the controller param-
46 eter tuning problem as a constrained optimization and integrate the different gait patterns as context
47 variables [3], (ii) we extend GOSAFEOPT [1] to the contextual case for which we give safety and opti-
48 mality guarantees. Furthermore, (iii) we demonstrate the superiority of contextual GOSAFEOPT over
49 other state-of-the-art safe exploration algorithms in simulation, and (iv) we show that GOSAFEOPT
50 successfully and safely tunes feedback control policies over two different gaits directly on the hard-
51 ware. To the best of our knowledge, we are the first to extend GOSAFEOPT to the contextual case
52 and to apply it to a highly dynamic and complex real-world system like the *Unitree Go1*.

53 2 Related Work

54 **Bridging the reality gap in quadrupedal locomotion tasks** Several previous studies have
55 emphasized the importance of considering an actuator behavior and identifying the system latency
56 to successfully bridge the *reality gap* in legged robot systems [4, 5, 6]. These studies develop a
57 simulation model of a legged robot system, incorporate either modeled or learned actuator dynamics
58 and train a control policy that can be effectively deployed to the robot hardware.

59 Incorporating this strategy into a model-based control framework is an area of active investigation.
60 In a model-based control regime, it’s typically more straightforward to introduce adjustable control
61 gain parameters and fine-tune them to align with the real-world behaviors of the robot. For instance,
62 Kim et al. [7], Kang et al. [8] use joint position- and velocity-level feedback to joint torque command
63 in order to address any discrepancy between the actual torque output and the intended torque
64 command for robots with proprioceptive actuators [9]. However, the fine-tuning of these parameters
65 continues to present a significant challenge. Schperberg et al. [10] utilize the unscented Kalman
66 filter algorithm to recursively tune control parameters of a model-based motion controller online,
67 and they successfully demonstrate it on the simulated quadrupedal robot in the presence of sensor
68 noise and joint-level friction. However, their proposed tuning method is inherently unsafe and can
69 therefore lead to arbitrary harmful interactions with the system. In contrast, our method is evaluated
70 on hardware and generalizes to multiple gaits while avoiding any unsafe interactions with the robot.

71 **Safe exploration for controller parameter tuning** Training a controller directly on hardware
72 is a challenging task, as it requires sample efficient and safe exploration to avoid possible damage to
73 the robot. In such a context, Bayesian optimization (BO [11]) emerges as a suitable framework due
74 to its sample efficiency. A notable example in the field of legged robotics comes from Calandra et al.
75 [12], who successfully employed BO to learn optimal gait parameters for a bipedal robot platform
76 using data obtained from hardware experiments.

77 BO methods can be easily adapted to constrained settings for safe learning. Gelbart et al. [13],
78 Hernández-Lobato et al. [14], Marco et al. [15] utilize constrained BO for finding safe optimal con-
79 troller parameters. However, these works do not provide safety assurance during exploration. In con-
80 trast, methods such as SAFEOPT [16, 17] and its extensions [18, 19, 20, 1] guarantee safety throughout
81 the entire learning and exploration phases. Starting from an initial safe controller, SAFEOPT lever-
82 ages regularity properties of the underlying optimization to expand the set of safe controllers. This
83 expansion is inherently local, and accordingly SAFEOPT can miss the global optimum. For dynamical
84 systems, Baumann et al. [20] propose GOSAFE, a *global* safe exploration algorithm. GOSAFE altern-
85 ates between local safe exploration, where it also learns safe backup policies, and global exploration,
86 where it uses the learned backup policies to guarantee safety. Therefore, whereas SAFEOPT might be
87 restricted to a local optimum, GOSAFE can find the global one. However, the BO routine proposed
88 in GOSAFE is expensive and sample inefficient for all but low dimensional systems [1]. To this
89 end, Sukhija et al. [1] introduce GOSAFEOPT. GOSAFEOPT leverages the underlying Markovian

90 structure of the dynamical system to overcome GOSAFE’s restrictions. As a result, GOSAFEOPT
 91 can perform global safe exploration for realistic and high-dimensional dynamical systems.

92 We extend GOSAFEOPT by incorporating a contextual setting and apply it to a quadruped robot.
 93 In this application, we optimize the controller parameters for various gait patterns. It’s important
 94 to highlight that this domain is considerably high-dimensional, involving a twenty-four-dimensional
 95 state space, six-dimensional parameter space, and five-dimensional context space.

96 3 Problem Setting

97 **Safe learning formulation** The dynamics of robotic systems can generally be described as an
 98 ordinary differential equation (ODE) of the form $\dot{\mathbf{x}} = \mathbf{f}(\mathbf{x}, \mathbf{u})$ where $\mathbf{u} \in \mathcal{U} \subset \mathbb{R}^{d_u}$ is the control
 99 signal and $\mathbf{x} \in \mathcal{X} \subset \mathbb{R}^{d_x}$ is the generalized robot state. Due to the reality gap, disparities can arise
 100 between the real-world dynamics and the dynamics model \mathbf{f} . This often results in a significant
 101 divergence between the behaviors of models and actual real-world systems, thereby making the
 102 control of intricate and highly dynamic entities like quadrupeds particularly challenging.

103 A common solution to this problem is using a feedback policy to rectify the model inaccuracies. Given
 104 a desired input signal \mathbf{u}^* , desired state \mathbf{x}^* , and true system state \mathbf{x} , we formulate a parameterized
 105 feedback controller in the form $\mathbf{u} = \pi_{\theta}(\mathbf{u}^*, \mathbf{x}^*, \mathbf{x})$ that steers \mathbf{x} to closely align with \mathbf{x}^* . The
 106 parameters θ are picked to minimize the tracking error. A common example of such a feedback
 107 policy is PD control, where $\mathbf{u} = \mathbf{u}^* + \theta[(\mathbf{x}^* - \mathbf{x})^\top, (\mathbf{x}^* - \dot{\mathbf{x}})^\top]^\top$, where $\theta \in \mathbb{R}^{d_u \times 2d_x}$ corresponds
 108 to the controller gains. Typically, choosing the parameters θ involves a heuristic process, requiring
 109 experimental iterations with the physical hardware. However, such interactions can be unpredictably
 110 risky and could possibly cause damage to the hardware.

111 In this work, we formalize the tuning process as a constrained optimization problem:

$$\max_{\theta \in \Theta} g(\theta) \quad \text{such that } q_i(\theta) \geq 0, \forall i \in \mathcal{I}_q, \quad (1)$$

112 where g is an objective function, q_i are the constraints with $\mathcal{I}_q = \{1, \dots, c\}$, and Θ is a compact
 113 set of parameters over which we optimize. Since the true dynamics are unknown, we cannot solve
 114 Equation (1) directly. Instead, we interact with the robot to learn $g(\theta)$ and $q_i(\theta)$, and solve the
 115 optimization problem in a black-box fashion. As we interact directly with the robot hardware, it is
 116 important that the learning process is sample-efficient and safe, i.e., constraints q_i are not violated
 117 during learning. To this end, we use the model-free safe learning algorithm GOSAFEOPT.

118 **Extension to multiple gait patterns** We expand the applicability of our method to support a range
 119 of quadrupedal gait patterns and enable smooth online transitions among them. Each specific gait
 120 pattern demonstrates unique dynamic properties, therefore, the optimal feedback parameters θ vary
 121 depending on the gait pattern in question. We consider gaits as *contexts* \mathbf{z} from a (not necessarily
 122 finite) set of contexts \mathcal{Z} [3]. Contexts are essentially external variables specified by the user and
 123 remain untouched by the optimization process. We broaden our initial problem formulation from
 124 Equation (1) to include these contexts;

$$\max_{\theta \in \Theta} g(\theta, \mathbf{z}) \quad \text{such that } q_i(\theta, \mathbf{z}) \geq 0, \forall i \in \mathcal{I}_q, \quad (2)$$

125 where $\mathbf{z} \in \mathcal{Z}$ is the context, which in our scenario, is the gait pattern of interest.

126 It is noteworthy that the prior work by Sukhija et al. [1] only introduces GOSAFEOPT for the
 127 non-contextual setting. In this work, we extend it to the contextual case and give safety as well as
 128 optimality guarantees.

129 3.1 Assumptions

130 In this section, we reiterate the assumptions from Sukhija et al. [1] for GOSAFEOPT.

131 **Assumption 1** (Initial safe seed). *For any episode $n \geq 1$ with (user-specified) context $\mathbf{z}_n \in \mathcal{Z}$, a*
 132 *non-empty initial safe set of parameters $\mathcal{S}_{n-1}(\mathbf{z}_n) \subset \Theta$ is known. That is, for all $\theta \in \mathcal{S}_{n-1}(\mathbf{z}_n)$ and*
 133 *all $i \in \mathcal{I}_q$, $q_i(\theta, \mathbf{z}_n) \geq 0$.*

134 Here, $\mathcal{S}_n(\mathbf{z}) \supseteq \mathcal{S}_0(\mathbf{z})$ denotes the safe set after episode n for the given context \mathbf{z} as defined in
 135 Equation (14) in Appendix A. Given the prior knowledge of the dynamics, a conservative safe set
 136 of parameters represents some initial stable feedback controller. Accordingly, this assumption is
 137 typically satisfied in practice. The assumption is necessary as, in principle, during each iteration, an
 138 adversarial context could be chosen for which the initial safe set does not include any safe parameters.

139 **Assumption 2** (Continuity of objective and constraints). *Let h be defined as*

$$h(\boldsymbol{\theta}, \mathbf{z}, i) = \begin{cases} g(\boldsymbol{\theta}, \mathbf{z}) & \text{if } i = 0, \\ q_i(\boldsymbol{\theta}, \mathbf{z}) & \text{if } i \in \mathcal{I}_q. \end{cases} \quad (3)$$

140 *We assume that h lies in a reproducing kernel Hilbert space (RKHS) associated with a kernel k*
 141 *and has a bounded norm in that RKHS, that is, $\|h\|_k \leq B$. Furthermore, we assume that g and*
 142 *q_i ($\forall i \in \mathcal{I}_q$) are Lipschitz-continuous with known Lipschitz constants.*

143 This is a common assumption in the model-free safe exploration literature [17, 20, 1]. Sukhija et al.
 144 [1] discuss the practical implications of this assumption in more detail.

145 **Assumption 3.** *We obtain noisy measurements of h with measurement noise i.i.d. σ -sub-Gaussian.*
 146 *Specifically, for a measurement y_i of $h(\boldsymbol{\theta}, \mathbf{z}, i)$, we have $y_i = h(\boldsymbol{\theta}, \mathbf{z}, i) + \epsilon_i$ with ϵ_i σ -sub-Gaussian*
 147 *for all $i \in \mathcal{I}$ where we write $\mathcal{I} = \{0, \dots, c\}$.*

148 **Assumption 4.** *We observe the state $\mathbf{x}(t)$ every Δt seconds. Furthermore, for any $\mathbf{x}(t)$ and*
 149 *$\rho \in [0, 1]$, the distance to $\mathbf{x}(t + \rho\Delta t)$ induced by any action is bounded by a known constant Ξ , that*
 150 *is, $\|\mathbf{x}(t + \rho\Delta t) - \mathbf{x}(t)\| \leq \Xi$.*

151 Assumption 4 is crucial to guarantee safety in continuous time even though the state is measured at
 152 discrete time instances. For highly dynamic systems, such as quadrupeds, the observation frequency
 153 is typically very high, e.g., 500 Hz - 1 kHz, and accordingly Ξ is small.

154 **Assumption 5.** *We assume that, for all $i \in \{1, \dots, c\}$, q_i is defined as the minimum of a state-*
 155 *dependent function \bar{q}_i along the trajectory starting in \mathbf{x}_0 with controller $\pi_{\boldsymbol{\theta}}$. Formally,*

$$q_i(\boldsymbol{\theta}, \mathbf{z}) = \min_{\mathbf{x}' \in \xi_{(\mathbf{x}_0, \boldsymbol{\theta}, \mathbf{z})}} \bar{q}_i(\mathbf{x}', \mathbf{z}), \quad (4)$$

156 *with $\xi_{(\mathbf{x}_0, \boldsymbol{\theta}, \mathbf{z})} = \{\mathbf{x}_0 + \int_0^t \mathbf{f}(\mathbf{x}(\tau), \pi_{\boldsymbol{\theta}}(\mathbf{x}(\tau), \mathbf{z})) d\tau \mid t \geq 0\}$ representing the trajectory of $\mathbf{x}(t)$*
 157 *under policy parameter $\boldsymbol{\theta}$ and context \mathbf{z} starting from \mathbf{x}_0 at time 0.*

158 Assumption 5 is an assumption on our choice of the constraint. Many common constraints, such as
 159 the minimum distance to an obstacle along a trajectory, satisfy this assumption.

160 4 GOSAFEOPT for Controller Optimization for Quadrupedal Locomotion

161 In this section, we first provide a brief overview of our model-based locomotion controller and the
 162 gait parameterization. Following this, we discuss GOSAFEOPT and its contextual extension, for
 163 which we provide safety and optimality guarantees.

164 4.1 Control Pipeline

165 **Model-based locomotion controller** Our locomotion controller utilizes a combination of the model
 166 predictive control (MPC) and the whole-body control (WBC) method following the previous work by
 167 Kim et al. [7], Kang et al. [8]. The MPC generates dynamically consistent base and foot trajectories
 168 by finding an optimal solution of a finite-horizon optimal control problem, using a simplified model.
 169 To convert these trajectories into joint-level control signals, we implement a WBC method that
 170 incorporates a more sophisticated dynamics model and takes into account the physical constraints of
 171 the robot. More specifically, we use a WBC formulation similar to the one presented by Kim et al. [7].
 172 This method calculates the desired generalized coordinates \mathbf{x}^{cmd} , speed $\dot{\mathbf{x}}^{\text{cmd}}$, and acceleration $\ddot{\mathbf{x}}^{\text{cmd}}$
 173 on a kinematic level while respecting task priority via the null-space projection [21]. Subsequently, it
 174 finds joint torque commands by solving a quadratic program that aligns with the desired generalized
 175 acceleration, adhering to the motion equations of the floating base and other physical constraints.
 176 For a more detailed explanation of the WBC formulation, the reader is referred to Appendix C.

177 We emphasize that the feed-forward torque commands by themselves fail to produce desired motion
 178 on the robot hardware due to model discrepancies. Particularly, we observed the actuator dynamics
 179 and joint friction, which are impractical to include in the system model, contribute significantly
 180 to this model mismatch. As a practical solution, we compute the final joint torque commands
 181 $\boldsymbol{\tau}^{\text{cmd}} = \boldsymbol{\tau} + \mathbf{k}_p(\mathbf{x}^* - \mathbf{x}) + \mathbf{k}_d(\dot{\mathbf{x}}^* - \dot{\mathbf{x}})$ and send them to the robot with the feedback gains
 182 $\mathbf{k}_p \in \mathbb{R}^{d_u \times d_x}$ and $\mathbf{k}_d \in \mathbb{R}^{d_u \times d_x}$.

183 **Gait parameterizations** We parameterize a quadrupedal gait pattern with $\mathbf{z}^g = [d^g, t_s^g, o_1^g, o_2^g, o_3^g]$,
 184 where d^g is the duty cycle for gate g , t_s^g is the stride duration and o_i^g are the offsets of legs two to four
 185 respectively. The duty cycle is defined as the contact duration divided by the stride duration. In general,
 186 the optimal feedback parameters $(\mathbf{k}_p^*, \mathbf{k}_d^*)$ change with the gait. We show this empirically in Section 5.

187 4.2 Contextual GOSAFEOPT

188 We model the unknown objective and constraint functions through Gaussian Process regression [22].
 189 To this end, given a dataset $\{\mathbf{v}_j, \mathbf{y}_j\}_{j \leq n}$, with $\mathbf{v}_j = (\boldsymbol{\theta}_j, \mathbf{z}_j)$ and the kernel k , we calculate a mean
 190 and uncertainty estimate of our function:

$$\begin{aligned} \mu_n(\mathbf{v}, i) &= \mathbf{k}_n^\top(\mathbf{v})(\mathbf{K}_n + \sigma^2 \mathbf{I})^{-1} \mathbf{y}_{n,i}, \\ \sigma_n^2(\mathbf{v}, i) &= k(\mathbf{v}, \mathbf{v}) - \mathbf{k}_n^\top(\mathbf{v})(\mathbf{K}_n + \sigma^2 \mathbf{I})^{-1} \mathbf{k}_n(\mathbf{v}), \end{aligned} \quad (5)$$

191 where $\mathbf{y}_{n,i} = [y_{j,i}]_{j \leq n}^\top$ are the observations of $h(\cdot, i)$, $\mathbf{k}_n(\mathbf{v}) = [k(\mathbf{v}, \mathbf{v}_j)]_{j \leq n}^\top$, and $\mathbf{K}_n =$
 192 $[k(\mathbf{v}_j, \mathbf{v}_l)]_{j,l \leq n}$ is the kernel matrix. We leverage these estimates to provide high-probability frequen-
 193 tist confidence intervals.

194 **Lemma 1** (Confidence intervals, Theorem 2 of [23] and Lemma 4.1 of [17]). *For any $\delta \in (0, 1)$ and*
 195 *under Assumptions 2 and 3, with probability at least $1 - \delta$ it holds jointly for all $n, i, \mathbf{z}, \boldsymbol{\theta}$ that*

$$|h(\boldsymbol{\theta}, \mathbf{z}, i) - \mu_n(\boldsymbol{\theta}, \mathbf{z}, i)| \leq \beta_n(\delta) \cdot \sigma_n(\boldsymbol{\theta}, \mathbf{z}, i) \quad (6)$$

196 with $\beta_n(\delta) \leq \mathcal{O}(B + 4\sigma\sqrt{2(\gamma_n|\mathcal{I}| + 1 + \log(1/\delta))})$ where

$$\gamma_n = \max_{\substack{A \subset \Theta \times \mathcal{Z} \times \mathcal{I} \\ |A| \leq n}} \mathbf{I}(\mathbf{y}_A; \mathbf{h}_A). \quad (7)$$

197 Here, $\mathbf{I}(\mathbf{y}_A; \mathbf{h}_A)$ denotes the *mutual information* between $\mathbf{h}_A = [h(\mathbf{v})]_{\mathbf{v} \in A}$, if modeled with a GP,
 198 and the noisy observations \mathbf{y}_A at \mathbf{h}_A , and it quantifies the reduction in uncertainty about h upon
 199 observing \mathbf{y}_A at points A . The quantity γ_n is a Bayesian construct, however, in the frequentist setting
 200 it quantifies the complexity of learning the function \mathbf{h} . It is instance dependent and can be bounded
 201 depending on the domain $\Theta \times \mathcal{Z} \times \mathcal{I}$ and kernel function k (see Appendix A).

202 Given the confidence interval from Equation (6), we define a confidence set for each context \mathbf{z} ,
 203 parameter $\boldsymbol{\theta}$ and index $0 \leq i \leq c$, as

$$C_0(\boldsymbol{\theta}, \mathbf{z}, i) = \begin{cases} [0, \infty] & \text{if } \boldsymbol{\theta} \in \mathcal{S}_0(\mathbf{z}) \text{ and } i \geq 1, \\ [-\infty, \infty] & \text{otherwise,} \end{cases} \quad (8)$$

$$C_n(\boldsymbol{\theta}, \mathbf{z}, i) = C_{n-1}(\boldsymbol{\theta}, \mathbf{z}, i) \cap [\mu_n(\boldsymbol{\theta}, \mathbf{z}, i) \pm \beta_n(\delta) \cdot \sigma_n(\boldsymbol{\theta}, \mathbf{z}, i)], \quad (9)$$

204 We refer to $l_n(\boldsymbol{\theta}, \mathbf{z}, i) = \min C_n(\boldsymbol{\theta}, \mathbf{z}, i)$ as the lower bound, $u_n(\boldsymbol{\theta}, \mathbf{z}, i) = \max C_n(\boldsymbol{\theta}, \mathbf{z}, i)$ the
 205 upper bound, and $w_n(\boldsymbol{\theta}, \mathbf{z}, i) = u_n(\boldsymbol{\theta}, \mathbf{z}, i) - l_n(\boldsymbol{\theta}, \mathbf{z}, i)$ the width of our confidence set.

206 4.2.1 Algorithm

207 An episode n of contextual GOSAFEOPT with the given (user-specified) context $\mathbf{z}_n \in \mathcal{Z}$ is performed
 208 in one of two alternating stages: *local safe exploration* (LSE) and *global exploration* (GE).

209 **Local safe exploration** During the LSE stage, we explore the subset of the parameter space
 210 Θ which is known to be safe, and learn backup policies for each visited state. In this stage, the
 211 parameters are selected according to the acquisition function

$$\boldsymbol{\theta}_n = \underset{\boldsymbol{\theta} \in \mathcal{G}_{n-1}(\mathbf{z}_n) \cup \mathcal{M}_{n-1}(\mathbf{z}_n)}{\text{argmax}} \max_{i \in \mathcal{I}} w_{n-1}(\boldsymbol{\theta}, \mathbf{z}_n, i) \quad (10)$$

212 where \mathbf{h} , $\mathcal{G}_n(\mathbf{z}_n) \subseteq S_n(\mathbf{z}_n)$ is a set of “expanders” (c.f., Equation (15) in Appendix A) and
 213 $\mathcal{M}_n(\mathbf{z}_n) \subseteq S_n(\mathbf{z}_n)$ is a set of “maximizers” (c.f., Equation (17) in Appendix A). Intuitively,
 214 $\mathcal{G}_n(\mathbf{z}_n) \cup \mathcal{M}_n(\mathbf{z}_n)$ represents those parameters that can potentially lead to an expansion of the safe
 215 set $S_n(\mathbf{z}_n)$ or potentially be a solution to the optimization problem of Equation (2) with context \mathbf{z}_n .

216 **Global exploration** If LSE converged (see Equation (20) in Appendix A), we run the GE stage
 217 where we evaluate possibly unsafe policies and trigger a backup policy whenever necessary. If no
 218 backup policy is triggered, we conclude that the evaluated policy is safe and add it to our safe set.
 219 After a new parameter is added to the safe set during GE, we continue with LSE.

220 The parameters are selected according to the acquisition function

$$\boldsymbol{\theta}_n = \underset{\boldsymbol{\theta} \in \Theta \setminus (S_{n-1}(\mathbf{z}_n) \cup \mathcal{E}(\mathbf{z}_n))}{\operatorname{argmax}} \max_{i \in \mathcal{I}} w_{n-1}(\boldsymbol{\theta}, \mathbf{z}_n, i) \quad (11)$$

221 where \mathcal{E} denotes all parameters which have been shown to be unsafe (see line 7 of Algorithm 4 in
 222 Appendix A). If all parameters have been determined as either safe or unsafe, i.e., $\Theta \setminus (S_n(\mathbf{z}_n) \cup$
 223 $\mathcal{E}(\mathbf{z}_n)) = \emptyset$, then GE has converged.

224 **Summary** A detailed description of the contextual GOSAFEOPt algorithm is provided in Ap-
 225 pendix A.2. GOSAFEOPt alternates between local safe exploration and global exploration. Therefore,
 226 it can seek for the optimum globally. We provide an example in Figure 4 in Appendix B.

227 The only difference between the contextual and non-contextual variants is that contextual
 228 GOSAFEOPt maintains separate sets $S_n, C_n, \mathcal{B}_n, \mathcal{D}_n, \mathcal{E}$, and $\mathcal{X}_{\text{Fail}}$ for each context $\mathbf{z} \in \mathcal{Z}$. For
 229 any given context $\mathbf{z} \in \mathcal{Z}$, the running best guess of contextual GOSAFEOPt for the optimum is
 230 $\hat{\boldsymbol{\theta}}_n(\mathbf{z}) = \operatorname{argmax}_{\boldsymbol{\theta} \in S_n(\mathbf{z})} l_n(\boldsymbol{\theta}, \mathbf{z}, 0)$.

231 4.2.2 Theoretical Results

232 In the following, we state our main theorem, which extends the safety and optimality guarantees from
 233 Sukhija et al. [1] to the contextual case.

234 We say that the solution to Equation (2), $\boldsymbol{\theta}^*(\mathbf{z})$, is *discoverable* if there exists a finite \tilde{n} such that
 235 $\boldsymbol{\theta}^*(\mathbf{z}) \in \bar{R}_\epsilon^{\mathbf{z}}(S_{\tilde{n}}(\mathbf{z}))$. Here, $\bar{R}_\epsilon^{\mathbf{z}}(S) \subseteq \Theta$ represents the largest safe set which can be reached safely
 236 from $S \subseteq \Theta$ up to ϵ -precision (c.f., Equation (19) in Appendix A).

237 **Theorem 1.** Consider any $\epsilon > 0$ and $\delta \in (0, 1)$. Further, let Assumptions 1 to 5 hold and $\beta_n(\delta)$ be
 238 defined as in Lemma 1. For any context $\mathbf{z} \in \mathcal{Z}$, let $\tilde{n}(\mathbf{z})$ be the smallest integer such that

$$\frac{n(\mathbf{z})}{\beta_{\tilde{n}(\mathbf{z})}(\delta) \cdot \gamma_{n(\mathbf{z})|\mathcal{I}}(\mathbf{z})} \geq \frac{C|\Theta|^2}{\epsilon^2} \quad \text{where} \quad n(\mathbf{z}) = \sum_{n=1}^{\tilde{n}(\mathbf{z})} \mathbb{1}\{\mathbf{z} = \mathbf{z}_n\} \quad (12)$$

239 and $C = 32/\log(1 + \sigma^{-2})$. Here, $\gamma_n(\mathbf{z}) = \max_{A \subset \Theta \times \mathcal{I}, |A| \leq n} \mathbb{I}(\mathbf{y}_{A,\mathbf{z}}; \mathbf{h}_{A,\mathbf{z}}) \leq \gamma_n$ denotes the
 240 mutual information between $\mathbf{h}_{A,\mathbf{z}} = [h(\boldsymbol{\theta}, \mathbf{z}, i)]_{(\boldsymbol{\theta}, i) \in A}$ and corresponding observations.

241 Then, when running contextual GOSAFEOPt and if $\boldsymbol{\theta}^*(\mathbf{z})$ is discoverable, the following inequalities
 242 jointly hold with probability at least $1 - 2\delta$:

243 1. $\forall t \geq 0, i \in \mathcal{I}_q: \bar{q}_i(\mathbf{x}(t), \mathbf{z}) \geq 0, \quad (\text{safety})$

244 2. $\forall \mathbf{z} \in \mathcal{Z}, n \geq \tilde{n}(\mathbf{z}): g(\hat{\boldsymbol{\theta}}_n(\mathbf{z}), \mathbf{z}) \geq g(\boldsymbol{\theta}^*(\mathbf{z}), \mathbf{z}) - \epsilon. \quad (\text{optimality})$

245 It is natural to start for each $i \in \mathcal{I}$ with kernels $k_i^{\mathcal{Z}}$ and k_i^{Θ} on the space of contexts and the space of
 246 parameters, respectively, and to construct composite kernels $k_i = k_i^{\mathcal{Z}} \otimes k_i^{\Theta}$ or $k_i = k_i^{\mathcal{Z}} \oplus k_i^{\Theta}$ as the
 247 product or sum of the pairs of kernels (see section 5.1 of [3]). In this case, the information gain γ_n is
 248 sublinear in n for common choices of kernels $k_i^{\mathcal{Z}}$ and k_i^{Θ} implying that $n^*(\mathbf{z})$ is finite.

249 The theorem is proven in Appendix A.3. Comparing to contextual SAFEOPt [17] which is only
 250 guaranteed to converge to safe optima in $\bar{R}_\epsilon^{\mathbf{z}}(S_0(\mathbf{z}))$, the global exploration steps of contextual
 251 GOSAFEOPt can also “discover” a safe optimum which was not reachable from the initial safe seed.

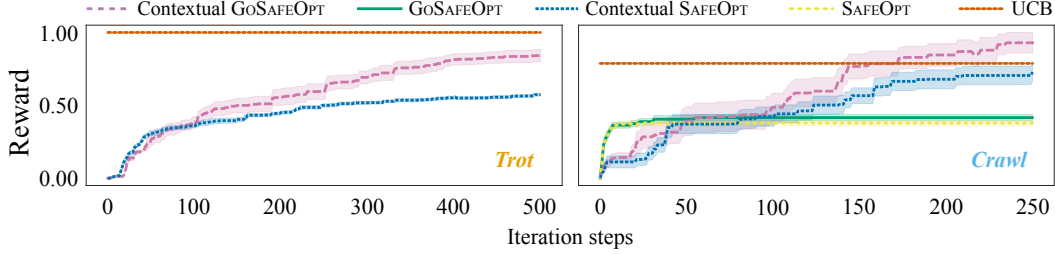


Figure 2: Simulation experiments. Left: Single context reward. GOSAFEOPT outperforms SAFEOPT on this task. On the right, we compare the learning curves of the contextual variants of GOSAFEOPT and SAFEOPT to the non-contextual ones for the *crawl* gait.

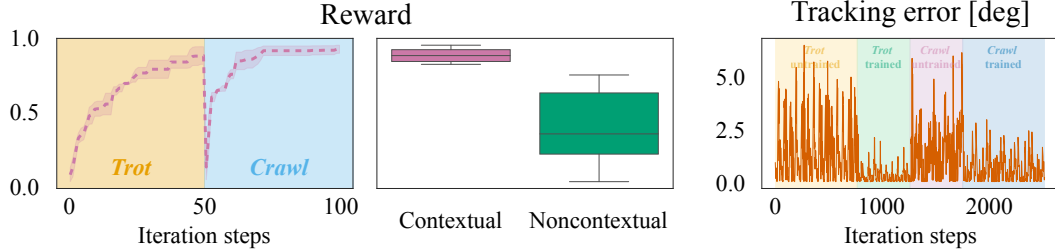


Figure 3: Hardware experiments. On the left, we present the learning curve of Contextual GOSAFEOPT. It shows that the algorithm successfully tunes the controller gains for *trot*, and then subsequently for *crawl*. In the middle, the performance of the optimized control gains of *trot* on *crawl* to the optimized gains for *crawl* is compared. On the right, we present the tracking error of the hip joint for the front-left leg with *trot* and *crawl* gait at initialization (*trot*: yellow, *crawl*: violet) and after optimization (*trot*: green, *crawl*: blue). We see that the optimized gaits give a drastic reduction in tracking error.

252 We remark that Theorem 1 is a worst-case result and, in particular, disregards a possible statistical
 253 dependence between different contexts. In practice, if a kernel is chosen which does not treat all
 254 contexts as independent, then the convergence can be much faster as knowledge about a particular
 255 context can be transferred to other contexts.

256 5 Experimental results

257 We evaluate contextual GOSAFEOPT on the *Unitree Go1* robot in both simulation and hardware. We
 258 provide a implementation, as well as a video of the simulation and hardware demonstrations in the
 259 supplementary. For both simulation and hardware, we use the following reward and constraints

$$g(\theta, z) = - \sum_{t \geq 0} \|\mathbf{x}^*(t) - \mathbf{x}(t, z, \theta)\|_{\mathbf{Q}_g}^2, \quad q_0(\theta, z) = \min_{t \geq 0} v_0 - \|\mathbf{x}^*(t) - \mathbf{x}(t, z, \theta)\|_{\mathbf{Q}_q}^2, \quad (13)$$

260 where \mathbf{Q}_g , and \mathbf{Q}_q are positive semi-definite matrices. More details on the reward are presented in
 261 Appendix D. As a feedback policy, we use the PD controller introduced in Section 4.1.

262 **Simulation experiments** In simulation, we compare contextual GOSAFEOPT to SAFEOPT, and
 263 GOSAFEOPT without contexts. Furthermore, we also evaluate GP-UCB [24], an unconstrained BO
 264 algorithm. To induce the ‘sim-to-real-gap’, we modify the simulation dynamics by adding additional
 265 disturbances to the system in the form of joint impedances at each joint (see Appendix D). The
 266 disturbances we induce can destabilize the system and thus cause constraint violation. Accordingly,
 267 we start all our experiments with a safe initial yet suboptimal feedback controller.

268 We optimize the controller for two different gaits; *trot*, and *crawl* sequentially. The parameters for the
 269 feedback controller and the parameterization of the gaits result in an overall model dimensionality
 270 of thirteen. We run all simulation experiments for ten different seeds and report the mean with one
 271 standard error. During all our experiments, we observe that all of the safe algorithms do not violate
 272 any safety constraint, while the standard GP-UCB method results in average constraint violation

273 for 4.7% and 8% of all evaluations for *trot* and *crawl* gait, respectively. In Figure 2, we compare
274 the normalized performance of GOSAFEOPT and SAFEOPT w.r.t. our objective for *trot* gait. It
275 is visible from the figure that GOSAFEOPT’s global exploration helps in finding better controller
276 parameters faster. Moreover, the GOSAFEOPT performs nearly as well as GP-UCB, while violating
277 no constraints. We also compare the contextual variants of GOSAFEOPT and SAFEOPT to the
278 non-contextual ones. From the figure, we conclude that contextual variants find better optima, with
279 contextual GOSAFEOPT finding the best one. We believe this is because the contextual variants
280 leverage the information collected while optimizing for *trot* gait, to find better optima for the *crawl*
281 gait, and also avoid unsafe/unstable evaluations unlike GP-UCB.

282 **Hardware Experiments** We also evaluate contextual GOSAFEOPT on the *Unitree Go1* robot. The
283 robot has twelve motors in total. Even though we have a good model of the robot dynamics, the
284 motors are typically difficult to model sufficiently accurately. Accordingly, we compensate for model
285 imprecisions using controller gains. To this end, for motors in the same positions of each leg (e.g.,
286 motors on the hip joint) we use the same gains. In total, we have a six-dimensional parameter space.

287 Similar to the simulation experiments, we first tune the controller for *trot* gait and then for the *crawl*
288 gait. We run the experiment over three different seeds and report the mean performance with one
289 standard error. In all our experiments, GOSAFEOPT results in zero constraint violations. Figure
290 3 show that GOSAFEOPT is able to safely fine-tune the feedback control parameters of both contexts.

291 Since each gait has different dynamic properties, the best solution for one gait may not generalize well
292 to other gaits. In Figure 3, in the middle, we depict how the best-performing parameters of *trot* gait do
293 not generalize to the *crawl* gait, and learning the *crawl* context increases the reward by a considerable
294 amount. From this, we conclude, that different gait patterns necessitate different controller gains.

295 Finally, in Figure 3, we also report the tracking performance of the tuned controller on the right.
296 Moreover, we compare for both *trot* and *crawl* gaits the tracking performance of the initial and
297 the tuned controller for the hip joint. We clearly see in the figure that the tuned controller makes
298 considerably less tracking error. We provide the error plots for the remaining joints in Appendix D.

299 6 Conclusion

300 We have extended GOSAFEOPT to incorporate the contextual setting and analyzed its convergence
301 and safety properties theoretically. We showcased the efficacy of our algorithm through its application
302 in adjusting the control parameters of a quadrupedal locomotion controller, in both simulation and
303 hardware experiments. The use of contextual information enhances the convergence for new gait
304 patterns by leveraging data from previously learned gaits. Furthermore, simulation results verify that
305 GOSAFEOPT can globally discover new safe regions without violating safety constraints. Across all
306 of our experiments, GOSAFEOPT outperforms prior approaches by a large margin and successfully
307 finds optimal control parameters for different quadrupedal gait patterns. We highlight that the
308 applicability of our proposed algorithm extends beyond our current scenario. It can be utilized to
309 fine-tune any feedback controllers on actual hardware systems, making it an effective strategy to
310 bridge the reality gap across various settings. For instance, we are interested in applying this method
311 to a more diverse set of quadrupedal gait patterns and extend its scope to encompass non-periodic
312 and unstructured gait patterns.

313 **Limitations** Even though the algorithm has theoretical safety guarantees, it is not always clear in
314 practice if all theoretical assumptions are met. For instance, even though the surrogate model might be
315 Lipschitz-continuous, the Lipschitz constant is generally not known a priori, i.e., Assumption 2 may
316 not be satisfied. This often results in a too conservative choice of parameters, e.g., small lengthscales
317 of the GP. Furthermore, a wrong parameter choice for the backup prior can result in unsafe global
318 exploration or no global exploration at all. In general, safe exploration methods such as SAFEOPT
319 and GOSAFEOPT have been successfully applied on several practical domains [1, 18, 19, 25, 26, 27],
320 however closing the gap between theory and practice is still actively being researched [28, 29, 30].

References

- [1] B. Sukhija, M. Turchetta, D. Lindner, A. Krause, S. Trimpe, and D. Baumann. Gosafeopt: Scalable safe exploration for global optimization of dynamical systems. *Artificial Intelligence*, 2023.
- [2] Unitree Robotics. <https://www.unitree.com/en/go1>.
- [3] A. Krause and C. Ong. Contextual gaussian process bandit optimization. In *Advances in Neural Information Processing Systems*, 2011.
- [4] J. Tan, T. Zhang, E. Coumans, A. Iscen, Y. Bai, D. Hafner, S. Bohez, and V. Vanhoucke. Sim-to-real: Learning agile locomotion for quadruped robots. In *Proceedings of Robotics: Science and Systems*, 2018.
- [5] J. Hwangbo, J. Lee, A. Dosovitskiy, D. Bellicoso, V. Tsounis, V. Koltun, and M. Hutter. Learning agile and dynamic motor skills for legged robots. *Science Robotics*, 2019.
- [6] D. Kang, J. Cheng, M. Zamora, F. Zargarbashi, and S. Coros. Rl + model-based control: Using on-demand optimal control to learn versatile legged locomotion, 2023.
- [7] D. Kim, J. D. Carlo, B. Katz, G. Bledt, and S. Kim. Highly dynamic quadruped locomotion via whole-body impulse control and model predictive control, 2019.
- [8] D. Kang, F. De Vincenti, N. C. Adami, and S. Coros. Animal motions on legged robots using nonlinear model predictive control. In *2022 IEEE/RSJ International Conference on Intelligent Robots and Systems (IROS)*. IEEE, 2022.
- [9] P. M. Wensing, A. Wang, S. Seok, D. Otten, J. Lang, and S. Kim. Proprioceptive actuator design in the mit cheetah: Impact mitigation and high-bandwidth physical interaction for dynamic legged robots. *IEEE Transactions on Robotics*, 2017.
- [10] A. Schperberg, S. D. Cairano, and M. Menner. Auto-tuning of controller and online trajectory planner for legged robots. *IEEE Robotics and Automation Letters*, 2022.
- [11] J. Mockus, V. Tiesis, and A. Zilinskas. The application of Bayesian methods for seeking the extremum. *Towards Global Optimization*, 1978.
- [12] R. Calandra, A. Seyfarth, J. Peters, and M. P. Deisenroth. Bayesian optimization for learning gaits under uncertainty: An experimental comparison on a dynamic bipedal walker. *Annals of Mathematics and Artificial Intelligence*, 2016.
- [13] M. Gelbart, J. Snoek, and R. Adams. Bayesian optimization with unknown constraints. *Conference on Uncertainty in Artificial Intelligence*, 2014.
- [14] J. M. Hernández-Lobato, M. A. Gelbart, R. P. Adams, M. W. Hoffman, and Z. Ghahramani. A general framework for constrained Bayesian optimization using information-based search. *The Journal of Machine Learning Research*, 2016.
- [15] A. Marco, D. Baumann, M. Khadiv, P. Hennig, L. Righetti, and S. Trimpe. Robot learning with crash constraints. *IEEE Robotics and Automation Letters*, 2021.
- [16] Y. Sui, A. Gotovos, J. Burdick, and A. Krause. Safe exploration for optimization with Gaussian processes. In *International Conference on Machine Learning*, 2015.
- [17] F. Berkenkamp, A. Krause, and A. P. Schoellig. Bayesian optimization with safety constraints: safe and automatic parameter tuning in robotics. *Machine Learning*, 2021.
- [18] Y. Sui, V. Zhuang, J. Burdick, and Y. Yue. Stagewise safe Bayesian optimization with Gaussian processes. In *International Conference on Machine Learning*, 2018.

- 363 [19] C. König, M. Turchetta, J. Lygeros, A. Rupenyan, and A. Krause. Safe and efficient model-free
364 adaptive control via bayesian optimization. In *IEEE International Conference on Robotics and*
365 *Automation*, 2021.
- 366 [20] D. Baumann, A. Marco, M. Turchetta, and S. Trimpe. GoSafe: Globally optimal safe robot
367 learning. In *IEEE International Conference on Robotics and Automation*, 2021. Proofs in
368 extended online version: arXiv 2105.13281.
- 369 [21] B. Siciliano, L. Sciavicco, L. Villani, and G. Oriolo. *Robotics: Modelling, Planning and Control*.
370 Springer Publishing Company, Incorporated, 1st edition, 2008.
- 371 [22] C. E. Rasmussen and C. K. I. Williams. *Gaussian Processes for Machine Learning (Adaptive*
372 *Computation and Machine Learning)*. The MIT Press, 2005.
- 373 [23] S. R. Chowdhury and A. Gopalan. On kernelized multi-armed bandits. In *International*
374 *Conference on Machine Learning*, 2017.
- 375 [24] N. Srinivas, A. Krause, S. M. Kakade, and M. Seeger. Gaussian process optimization in the
376 bandit setting: No regret and experimental design. *arXiv preprint arXiv:0912.3995*, 2009.
- 377 [25] A. Wischnewski, J. Betz, and B. Lohmann. A model-free algorithm to safely approach the
378 handling limit of an autonomous racecar. In *IEEE International Conference on Connected*
379 *Vehicles and Expo*, 2019.
- 380 [26] M. Fiducioso, S. Curi, B. Schumacher, M. Gwerder, and A. Krause. Safe contextual Bayesian
381 optimization for sustainable room temperature PID control tuning. In *International Joint*
382 *Conference on Artificial Intelligence*, 2019.
- 383 [27] S. E. Cooper and T. I. Netoff. Multidimensional bayesian estimation for deep brain stimulation
384 using the safeopt algorithm. *medRxiv*, 2022.
- 385 [28] C. Fiedler, C. W. Scherer, and S. Trimpe. Practical and rigorous uncertainty bounds for Gaussian
386 process regression. *AAAI Conference on Artificial Intelligence*, 35(8), 2021.
- 387 [29] F. Berkenkamp, A. P. Schoellig, and A. Krause. No-regret bayesian optimization with unknown
388 hyperparameters. *Journal of Machine Learning Research*, 2019.
- 389 [30] J. Rothfuss, C. Koenig, A. Rupenyan, and A. Krause. Meta-learning priors for safe bayesian
390 optimization. *arXiv preprint arXiv:2210.00762*, 2022.
- 391 [31] S. Vakili, K. Khezeli, and V. Picheny. On information gain and regret bounds in gaussian
392 process bandits. In *International Conference on Artificial Intelligence and Statistics*, 2021.
- 393 [32] G. Brockman, V. Cheung, L. Pettersson, J. Schneider, J. Schulman, J. Tang, and W. Zaremba.
394 Openai gym. *arXiv preprint arXiv:1606.01540*, 2016.
- 395 [33] D. Kang, F. De Vincenti, and S. Coros. Nonlinear model predictive control for quadrupedal
396 locomotion using second-order sensitivity analysis, 2022.
- 397 [34] K. Serkan, I. Turker, and G. Moncef. *Multidimensional particle swarm optimization for machine*
398 *learning and pattern recognition*. Springer-Verlag Berlin Heidelberg, 2014.
- 399 [35] Constrained Bayesian optimization with particle swarms for safe adaptive controller tuning.
400 *IFAC-PapersOnLine*, 2017.
- 401 [36] G. Pleiss, J. R. Gardner, K. Q. Weinberger, and A. G. Wilson. Constant-time predictive
402 distributions for gaussian processes. *arXiv: 1803.06058*, abs/1803.06058, 2018.

403	Contents of Appendix	
404	A Proofs	12
405	A.1 Definitions	12
406	A.2 Algorithm	12
407	A.3 Proof of Theorem 1	13
408	B Comparison of SAFEOPT and GOSAFEOPT	15
409	C Control Formulation	15
410	D Experimental Details	17
411	D.1 Bayesian optimization	17
412	D.2 Simulation	17
413	D.3 Hardware	17
414	E Practical modifications	17
415	E.1 Boundary conditions	17
416	E.2 Optimization	18
417	E.3 Fix iterations and discard unpromising new detected safe regions	19
418	E.4 Posterior estimation	19

419 **A Proofs**

420 **A.1 Definitions**

421 We begin by re-stating definitions of sets used by GOSAFE_{OPT} from Sukhija et al. [1] with an
422 additional context variable.

423 Fix an arbitrary context $\mathbf{z} \in \mathcal{Z}$. The *safe set* is defined recursively as

$$S_n(\mathbf{z}) = \bigcap_{i \in \mathcal{I}_q} \bigcup_{\theta' \in S_{n-1}(\mathbf{z})} \{\theta \in \Theta \mid l_n(\theta', \mathbf{z}, i) - L_\Theta(\mathbf{z}) \|\theta - \theta'\| \geq 0\} \quad (14)$$

424 where $L_\Theta(\mathbf{z})$ is the joint Lipschitz constant of g and the constraints q_i under context \mathbf{z} . The *expanders*
425 are defined as

$$\mathcal{G}_n(\mathbf{z}) = \{\theta \in S_n(\mathbf{z}) \mid e_n(\theta, \mathbf{z}) > 0\} \quad \text{with} \quad (15)$$

$$e_n(\theta, \mathbf{z}) = |\{\theta' \in \Theta \setminus S_n(\mathbf{z}) \mid \exists i \in \mathcal{I}_q : u_n(\theta, \mathbf{z}, i) - L_\Theta(\mathbf{z}) \|\theta - \theta'\| \geq 0\}| \quad (16)$$

426 and the *maximizers* are defined as

$$\mathcal{M}_n(\mathbf{z}) = \{\theta \in S_n(\mathbf{z}) \mid u_n(\theta, 0) \geq \max_{\theta' \in S_n(\mathbf{z})} l_n(\theta', 0)\}. \quad (17)$$

427 The analysis requires the ϵ -slacked safe region $\bar{R}_\epsilon^z(S)$ given an initial safe seed $S \subseteq \Theta$, which is
428 defined recursively as

$$R_\epsilon^z(S) = S \cup \{\theta \in \Theta \mid \exists \theta' \in S \text{ such that } \forall i \in \mathcal{I}_q : q_i(\theta', \mathbf{z}) - \epsilon - L_\Theta(\mathbf{z}) \|\theta - \theta'\| \geq 0\}, \quad (18)$$

$$\bar{R}_\epsilon^z(S) = \lim_{n \rightarrow \infty} (R_\epsilon^z)^n(S) \quad (19)$$

429 where $(R_\epsilon^z)^n$ denotes the n th composition of R_ϵ^z with itself.

430 **A.2 Algorithm**

431 **A.2.1 Local Safe Exploration**

432 During LSE, we keep track for each context $\mathbf{z} \in \mathcal{Z}$ of a set of backup policies $\mathcal{B}(\mathbf{z}) \subseteq \Theta \times \mathcal{X}$ and
433 observations of \mathbf{h} , which we denote by $\mathcal{D}(\mathbf{z}) \subseteq \Theta \times \mathbb{R}^{|\mathcal{I}|}$. An LSE step is described formally in
434 Algorithm 1.

Algorithm 1 Local Safe Exploration (LSE)

Input: Current context \mathbf{z}_n , safe sets S , sets of backups \mathcal{B} , datasets \mathcal{D} , Lipschitz constants L_Θ

1: Recommend parameter θ_n with Equation (10)

2: Collect $\mathcal{R} = \bigcup_{k \in \mathbb{N}} \{(\theta_n, \mathbf{x}(k))\}$ and $h(\theta_n, \mathbf{z}_n, i) + \varepsilon_n$

3: $\mathcal{B}(\mathbf{z}_n) = \mathcal{B}(\mathbf{z}_n) \cup \mathcal{R}$, $\mathcal{D}(\mathbf{z}_n) = \mathcal{D}(\mathbf{z}_n) \cup \{(\theta_n, h(\theta_n, \mathbf{z}_n, i) + \varepsilon_n)\}$

4: Update sets $S(\mathbf{z})$, $\mathcal{G}(\mathbf{z})$, and $\mathcal{M}(\mathbf{z})$ for all $\mathbf{z} \in \mathcal{Z}$ ▷ Equations (14), (15) and (17)

Return: $S, \mathcal{B}, \mathcal{D}$

435 The LSE stage terminates for some given context $\mathbf{z} \in \mathcal{Z}$ when the connected safe set is fully explored
436 and the optimum within the safe set is discovered. This happens when the uncertainty among the
437 expanders and maximizers is less than ϵ and the safe set is not expanding

$$\max_{\theta \in \mathcal{G}_{n-1}(\mathbf{z}) \cup \mathcal{M}_{n-1}(\mathbf{z})} \max_{i \in \mathcal{I}} w_{n-1}(\theta, \mathbf{z}, i) < \epsilon \quad \text{and} \quad S_{n-1}(\mathbf{z}) = S_n(\mathbf{z}). \quad (20)$$

438 **A.2.2 Global Exploration**

439 A GE step conducts an experiment about a candidate parameter $\theta_n \in \Theta$ which may not be safe. If the
440 safety boundary is approached, GE conservatively triggers a safe backup policy. If, on the other hand,
441 the experiment is successful, a new (potentially disconnected) safe region was discovered which can
442 then be explored by LSE in the following steps. A GE step is described formally in Algorithm 2.

Algorithm 2 Global Exploration (GE)

Input: z_n , safe sets S , confidence intervals C , sets of backups \mathcal{B} , datasets \mathcal{D} , fail sets \mathcal{E} and $\mathcal{X}_{\text{Fail}}$

- 1: Recommend global parameter θ_n with Equation (11)
- 2: $\theta = \theta_n$, $\mathbf{x}_{\text{Fail}} = \emptyset$, Boundary = False
- 3: **while** Experiment not finished **do** ▷ Rollout policy
- 4: **if** Not Boundary **then**
- 5: Boundary, $\theta_s^* = \text{BOUNDARYCONDITION}(z_n, \mathbf{x}(k), \mathcal{B})$
- 6: **if** Boundary **then** ▷ Trigger backup policy
- 7: $\theta = \theta_s^*$, $\mathbf{x}_{\text{Fail}} = \mathbf{x}(k)$
- 8: $\mathcal{E} = \mathcal{E} \cup \{\theta_n\}$, $\mathcal{X}_{\text{Fail}} = \mathcal{X}_{\text{Fail}} \cup \{\mathbf{x}_{\text{Fail}}\}$ ▷ Update fail sets
- 9: Execute until $\mathbf{x}(k)$
- 10: Collect $\mathcal{R} = \bigcup_{k \in \mathbb{N}} \{(\theta_n, \mathbf{x}(k))\}$, and $h(\theta_n, z_n, i) + \varepsilon_n$
- 11: **if** Not Boundary **then** ▷ Successful global search
- 12: $\mathcal{B}(z_n) = \mathcal{B}(z_n) \cup \mathcal{R}$ and $\mathcal{D}(z_n) = \mathcal{D}(z_n) \cup \{(\theta_n, h(\theta_n, z_n, i) + \varepsilon_n)\}$
- 13: $S(z_n) = S(z_n) \cup \{\theta_n\}$
- 14: $C(\theta_n, z_n, i) = C(\theta_n, z_n, i) \cap [0, \infty]$ for all $i \in \mathcal{I}_q$

Return: $S, C, \mathcal{B}, \mathcal{D}, \mathcal{E}, \mathcal{X}_{\text{Fail}}$

443 **A.2.3 Boundary Condition**

444 The boundary condition checks when the system is in the state \mathbf{x} whether there is a backup $(\theta_s, \mathbf{x}_s) \in$
445 $\mathcal{B}(z)$ such that \mathbf{x}_s is sufficiently close to \mathbf{x} to guarantee that θ_s can steer the system back to safety
446 for any state which may be reached in the next time step. If no such backups exist for the next states,
447 a backup is triggered at the current state. In this case, the backup parameter θ_s^* with the largest safety
448 margin is triggered:

$$\theta_s^* = \max_{(\theta_s, \mathbf{x}_s) \in \mathcal{B}_n(z_n)} \min_{i \in \mathcal{I}_q} l_n(\theta_s, z_n, i) - L_x \|\mathbf{x} - \mathbf{x}_s\|. \quad (21)$$

Algorithm 3 BOUNDARYCONDITION

Input: context z_n , state \mathbf{x} , backups \mathcal{B}

- 1: **if** $\forall (\theta_s, \mathbf{x}_s) \in \mathcal{B}(z_n), \exists i \in \mathcal{I}_q : l_n(\theta_s, z_n, i) - L_x \|\mathbf{x} - \mathbf{x}_s\| + \Xi < 0$ **then**
- 2: Boundary = True, Calculate θ_s^* (Equation (21))
- 3: **else**
- 4: Boundary = False, $\theta_s^* = \text{Null}$

return: Boundary, θ_s^*

449 **A.2.4 Contextual GOSAFE OPT**

450 The algorithm stops for a particular context $z \in \mathcal{Z}$ when

$$\underbrace{\text{Equation (20) is satisfied}}_{\text{LSE converged}} \quad \text{and} \quad \underbrace{\Theta \setminus (S_n(z_n) \cup \mathcal{E}(z_n)) = \emptyset}_{\text{GE converged}}. \quad (22)$$

451 The full algorithm is described in Algorithm 4.

452 **A.3 Proof of Theorem 1**

453 *Proof.* We first derive the sample complexity bound of non-contextual GOSAFE OPT. Then, we
454 extend this sample complexity bound to contextual GOSAFE OPT. We assume without loss of
455 generality that β_n is monotonically increasing with n .

456 **Sample complexity** Assume first that the context is fixed, that is, $\forall n \geq 1 : z_n = z$. In this case,
457 the safety guarantee (with probability at least $1 - \delta$) follows directly from Theorem 4.1 of Sukhija

Table 1: Here we summarize different magnitudes of γ_n for composite kernels from Theorems 2 and 3 of Krause and Ong [3] and for individual kernels from Theorem 5 of Srinivas et al. [24] and Remark 2 of Vakili et al. [31]. The magnitudes hold under the assumption that the domain of the kernel is compact. γ^\ominus and $\gamma^\mathcal{Z}$ denote the information gain for the kernels k^\ominus and $k^\mathcal{Z}$, respectively. B_ν is the modified Bessel function.

Kernel	$k(\mathbf{v}, \mathbf{v}')$	γ_n
Product	$k^\ominus(\mathbf{v}, \mathbf{v}') \cdot k^\mathcal{Z}(\mathbf{v}, \mathbf{v}')$ if $k^\mathcal{Z}$ has rank at most d	$d\gamma_n^\ominus + d \log(n)$
Sum	$k^\ominus(\mathbf{v}, \mathbf{v}') + k^\mathcal{Z}(\mathbf{v}, \mathbf{v}')$	$\gamma_n^\ominus + \gamma_n^\mathcal{Z} + 2 \log(n)$
Linear	$\mathbf{v}^\top \mathbf{v}'$	$\mathcal{O}(d \log(n))$
RBF	$e^{-\frac{\ \mathbf{v}-\mathbf{v}'\ ^2}{2l^2}}$	$\mathcal{O}(\log^{d+1}(n))$
Matérn	$\frac{1}{\Gamma(\nu)2^{\nu-1}} \left(\frac{\sqrt{2\nu}\ \mathbf{v}-\mathbf{v}'\ }{l} \right)^\nu B_\nu \left(\frac{\sqrt{2\nu}\ \mathbf{v}-\mathbf{v}'\ }{l} \right)$	$\mathcal{O}\left(n^{\frac{d}{2\nu+d}} \log^{\frac{2\nu}{2\nu+d}}(n)\right)$

478 B Comparison of SAFEOPT and GOSAFEOPT

479 To visually analyze the different exploration properties of SAFEOPT and GOSAFEOPT we use
 480 the Pendulum Environment from OpenAI [32] as an example. The ideal trajectory is given by
 481 some undisturbed controller. In our toy problem, we use a simple PD control which is sufficient
 482 for the pendulum swing-up problem and various oscillating trajectories. To simulate the sim to
 483 hardware gap, we artificially add a disturbance to the applied torque in the form of joint impedances
 484 $\boldsymbol{\tau} = \boldsymbol{\tau}^* - \boldsymbol{\theta}_p^d(\mathbf{x}^* - \mathbf{x}) + \boldsymbol{\theta}_d^d\dot{\mathbf{x}}$ where $\boldsymbol{\theta}_p^d$ and $\boldsymbol{\theta}_d^d$ are unknown disturbance parameters and \mathbf{x}^* , \mathbf{x}
 485 are the desired and observed motor angles. We use GOSAFEOPT to tune an additional PD controller
 486 which should follow the ideal trajectory and compensate for the artificial disturbance. Figure 4 shows
 487 an example run of SAFEOPT and GOSAFEOPT. Whereas SAFEOPT is restricted to expanding the
 488 initial safe region, GOSAFEOPT can discover new safe regions, and thus find a better optimum.

489 C Control Formulation

490 Our model-based motion controller integrates the MPC and WBC methods to enhance both robustness
 491 and maneuverability. The MPC is responsible for generating base and foot trajectories, while the
 492 WBC converts these trajectories into joint-level commands. For the MPC component, we employ the
 493 model predictive control formulation proposed by Kang et al. [33, 8]. This formulation represents a
 494 finite-horizon optimal control problem as a nonlinear program utilizing the variable-height inverted
 495 pendulum model. The optimal solution of the nonlinear program is determined by using a second-
 496 order gradient-based method. For a more in-depth understanding of the MPC formulation, we direct
 497 readers to the prior work by Kang et al. [33, 8].

498 We employ a slight modification of the WBC formulation introduced by Kim et al. [7], adapting it
 499 to align with the MPC. Following the method proposed by Kim et al. [7], we compute the desired
 500 generalized coordinates \mathbf{x}^{cmd} , speed $\dot{\mathbf{x}}^{\text{cmd}}$, and acceleration $\ddot{\mathbf{x}}^{\text{cmd}}$ for a quadruped system at the
 501 kinematic level. This process involves translating desired task space (Cartesian space) positions,
 502 velocities, and accelerations into configuration space counterparts. Throughout this process, we
 503 enforce task priority through iterative null-space projection [21]. The top priority is assigned to the
 504 contact foot constraint task, followed by the base orientation tracking task. The base position tracking
 505 task is given the third priority, and the swing foot tracking task is assigned the final priority.

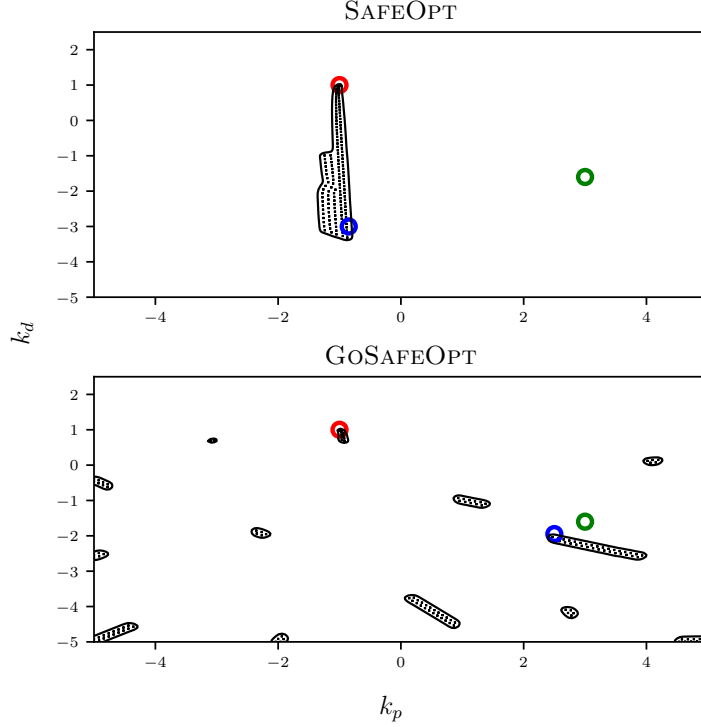


Figure 4: Example run of SAFEOPT and GOSAFEOPT. The red circle denotes the initial safe point. The black dots denote observed points. The green circle denotes the true safe optimum and the blue circle denotes the optimal point determined by SAFEOPT and GOSAFEOPT, respectively, after 150 iterations. The discovered safe sets are shown in black. GOSAFEOPT gets closer to the true optimum by discovering new safe regions which are not connected to the initial safe region.

506 Subsequently, we solve the following quadratic program:

$$\min_{\delta_{\ddot{x}}, \mathbf{f}_c} \|\delta_{\ddot{x}}\|_Q^2 \quad (26a)$$

$$\text{s.t.} \quad \mathbf{S}_f(\mathbf{M}\ddot{\mathbf{x}} + \mathbf{b} + \mathbf{g}) = \mathbf{S}_f \mathbf{J}_c^\top \mathbf{f}_c \quad (26b)$$

$$\ddot{\mathbf{x}} = \ddot{\mathbf{x}}^{\text{cmd}} + [\delta_{\ddot{x}}, \mathbf{0}_{n_j}]^\top \quad (26c)$$

$$\mathbf{W} \mathbf{f}_c \geq \mathbf{0}, \quad (26d)$$

507 where $\delta_{\ddot{x}}$ denotes a relaxation variables for the floating base acceleration and \mathbf{f}_c denotes contact
 508 forces with the contact Jacobian \mathbf{J}_c . Equation (26a) is the objective function that penalizes the
 509 weighted norm of $\delta_{\ddot{x}}$ with the weight matrix \mathbf{Q} . Equation (26b) corresponds to the equation of motion
 510 of the floating base, representing the first six rows of the whole-body equation of motion, with \mathbf{S}_f
 511 being the corresponding selection matrix. Lastly, Equation (26d) sets forth the Coulomb friction
 512 constraints. This procedure refines the desired generalized acceleration $\ddot{\mathbf{x}}^{\text{cmd}}$, which is calculated at
 513 the kinematic level, by incorporating the dynamic impacts of the robot's movements.

514 Upon determining $\ddot{\mathbf{x}}$ is determined, we compute the joint torque commands as follows:

$$\boldsymbol{\tau} = \mathbf{M}\ddot{\mathbf{x}} + \mathbf{b} + \mathbf{g} - \mathbf{J}_c^\top \mathbf{f}_c. \quad (27)$$

515 The final torque commands are calculated using $\boldsymbol{\tau}^{\text{cmd}} = \boldsymbol{\tau} + \mathbf{k}_p(\mathbf{x}^* - \mathbf{x}) + \mathbf{k}_d(\dot{\mathbf{x}}^* - \dot{\mathbf{x}})$ and dispatched
 516 to the robot with the feedback gains $\mathbf{k}_p \in \mathbb{R}^{d_u \times d_x}$ and $\mathbf{k}_d \in \mathbb{R}^{d_u \times d_x}$. As previously noted, this
 517 step is crucial in dealing with model mismatches, specifically, the differences in joint-level behavior
 518 stemming from actuator dynamics and joint friction.

519 D Experimental Details

520 D.1 Bayesian optimization

521 For all our experiments, we use a Matérn kernel with $\nu = 1.5$ for the underlying Gaussian Process.
 522 The lengthscales are fixed during the whole optimization process and set to

Table 2: Kernel lengthscales

	lengthscales
Simulation	[0.1, 0.05, 0.1, 0.05, 0.1, 0.05, 0.1, 0.05, 0.1, 0.1, 0.1, 0.1, 0.1]
Hardware	[0.3, 0.3, 0.3, 0.3, 0.3, 0.3, 0.5, 0.5, 0.5, 0.5, 0.5]

523 where the first n parameters correspond to the $(\mathbf{k}_p, \mathbf{k}_d)$ pairs and the last parameters to the context.
 524 For all experiments, we use $\beta = 16$ for the LCB on the constraints.

525 D.2 Simulation

526 **Disturbance model** The full body controller of the quadruped is artificially disturbed by changing
 527 the desired torque of each motor. More specifically, an artificial disturbance α_l is applied to each motor
 528 of the four legs l , resulting in an applied motor torque $\boldsymbol{\tau}_{\text{applied}}^{i,l} = \alpha_l \boldsymbol{\tau}_{\text{desired}}^{i,l} + \boldsymbol{\theta}_l [\mathbf{q}_{l,i}^* - \mathbf{q}_{l,i}, -\dot{\mathbf{q}}_{l,i}]^\top$
 529 for motors i of leg l .

530 **Reward function** The state $\mathbf{x} \in \mathbb{R}^{24}$ of all 12 motors is described by each motor angle and angular
 531 velocity. We set the matrices from Equation (13) to $\mathbf{Q}_g = \mathbf{I}^{24 \times 24}$ and $\mathbf{Q}_q^{i,j} = \mathbb{1}\{i = j \wedge i \leq 12\}$.

532 D.3 Hardware

533 We slightly modify the reward function for the hardware experiment and include a penalty term on
 534 the joint velocities.

$$\hat{g}(\boldsymbol{\theta}, \mathbf{z}) = g(\boldsymbol{\theta}, \mathbf{z}) - \|\mathbf{x}(t)\|_{\mathbf{Q}_p}^2$$

535 where the velocity state errors in \mathbf{Q}_g and \mathbf{Q}_q in Equation 13 are set to zero, since the observed
 536 joint velocities are noisy finite difference approximations of the joint angles. Furthermore, we
 537 define \mathbf{Q}_p to only include the noisy joint velocity observations. More specifically, we define
 538 $\mathbf{Q}_q^{i,j} = \mathbf{Q}_q^{i,j} = \mathbb{1}\{i = j \wedge i \leq 12\}$ and $\mathbf{Q}_p^{i,j} = \frac{1}{2} \mathbb{1}\{i = j \wedge i > 12\}$ and $\mathbf{Q}_g, \mathbf{Q}_q, \mathbf{Q}_p \in \mathbb{R}^{24 \times 24}$.
 539 Experimental results have shown, that adding a penalty term on the joint velocities acts as a regulator
 540 to prefer solutions where motor vibrations are low. This has shown to improve overall convergence
 541 and to visibly avoid solutions where motor vibrations are high.

542 The tracking performance is evaluated for the crawl gait before and after learning the optimal
 543 parameters for the motors 1-3 as shown in Figure 1. Figure 5 shows that the optimal feedback control
 544 parameters drastically reduce motor vibrations and increase the tracking performance.

545 E Practical modifications

546 E.1 Boundary conditions

547 We use the idea from Sukhija et al. [1] to reduce computational complexity by defining an interior and
 548 marginal set. Intuitively, the interior set contains all observed states for which the safety margin is
 549 high and the marginal set includes all states where the safety margin is greater than a certain threshold.
 550 More formally, Sukhija et al. [1] defines the interior and marginal set as :

$$\Omega_{I,n} = \{\mathbf{x}_s \in \mathcal{X} \mid (\boldsymbol{\theta}, \mathbf{x}_s) \in \mathcal{B}_n : \forall i \in \mathcal{I}_q, l_n(\boldsymbol{\theta}, i) \geq \eta_u\} \quad (28)$$

$$\Omega_{M,n} = \{\mathbf{x}_s \in \mathcal{X} \mid (\boldsymbol{\theta}, \mathbf{x}_s) \in \mathcal{B}_n : \forall i \in \mathcal{I}_q, \eta_l \leq l_n(\boldsymbol{\theta}, i) < \eta_u\} \quad (29)$$

Table 4: Swarmopt parameters

Parameter	Value	Description
Θ_g	1	Social coefficient
Θ_p	1	Cognitive coefficient
w	0.9	Inertial weight
n	100	Number of iterations
n_r	100	Number of restarts if no safe set is found

566 E.3 Fix iterations and discard unpromising new detected safe regions

567 In practice, it is not practical to fully explore a safe set before the global exploration phase. For our
568 experiments, the number of iterations for the local and global exploration phase are fixed to $n_l = 10$
569 and $n_g = 5$, respectively. To avoid exploring for all n_l steps in unpromising regions, we define
570 $n_d = 5 < n_l$ and switch to local exploration of the best set if the best reward estimation of the current
571 set is much less than the best global reward estimate. That is, we switch to the best set if $\hat{r}_i^* < c\hat{r}^*$
572 and $n_d = n_l$.

573 E.4 Posterior estimation

574 Each BO step requires the optimization of the GOSAFEOPTE acquisition function to predict the next
575 parameters to evaluate. This paper uses the standard particle swarm [34] algorithm, which requires the
576 computation of the posterior distribution at each optimization step for all particles. To speed up the
577 computation of the posterior distribution, the paper uses Lanczos Variance Estimates Pleiss et al. [36].